High resolution neutron scattering on ionic surfactant micelles : sds in water

B. Cabane, R. Duplessix, Thomas Zemb

J. Physique **46** (1985) 2161-2178 DÉCEMBRE **1985**, PAGE 2161

Classification
Physics Abstracts
61.12

High resolution neutron scattering on ionic surfactant micelles : SDS in water (*)

B. Cabane (++)

Laboratoire de Physique des Solides (+), Université Paris Sud, 91405 Orsay, France

R. Duplessix

Centre de Recherches sur les Macromolécules, 6, rue Boussingault, 67083 Strasbourg, France

and T. Zemb

Département de Physico-Chimie, CEN-Saclay, 91191 Gif-sur-Yvette, France

(*Reçu le 26 octobre 1984, accepté sous forme définitive le 25 juillet 1985*)

Résumé. — On améliore la résolution obtenue en diffusion des neutrons aux petits angles pour déterminer la structure des micelles de dodécylsulfate de sodium dans l'eau. L'expérience mesure la distribution moyenne des distances entre tous les noyaux d'une micelle, ainsi que les distributions de distances entre des groupes deutérés attachés aux positions ω et γ des chaînes de SDS. A basse résolution (15 Å) on n'observe que la structure moyenne de la micelle : il s'agit d'une sphère contenant $\bar{N} = 74$ molécules de SDS ; son cœur hydrocarboné a un rayon de 18,4 Å ; il contient très peu d'eau, en tout cas moins qu'une molécule d'eau par molécule de SDS. A haute résolution (5 Å) on voit surtout les fluctuations spontanées qui écartent la micelle de cette structure moyenne. Ces fluctuations produisent une dispersion des nombres d'agrégation ($\sigma^2/\bar{N}^2 = 0{,}1$) et des déviations par rapport à la forme sphérique. La structure interne du cœur, mesurée par les distances entre groupes deutérés, est également distordue par chacune de ces fluctuations : les queues de chaînes (ω) ne sont pas concentrées près d'un « centre », et les méthylènes en position γ ne restent pas dans une coquille sphérique.

Abstract. — An improvement over previous determinations of the structure of sodium dodecyl sulfate micelles has been obtained from small angle neutron scattering. The experiment measures the average distribution of distances between all nuclei within a micelle, and also those between deuterium labels attached at positions ω or γ on the SDS chains. At *low resolution* (15 Å), only the *average structure* of the micelle is observed : this is a dense sphere containing $\bar{N} = 74$ SDS molecules ; the hydrocarbon core has a radius of 18.4 Å and contains less than one water molecule per SDS molecule. At *high resolution* (5 Å), *fluctuations* away from the average structure are observed. If the internal structure of the core is not resolved, one sees mainly the dispersion in the aggregation numbers ($\sigma_N/\bar{N} = 0.33$) or radii ($\sigma_R/\bar{R} = 0.1$) of the micelle. When the distributions of distances between deuterium labels are observed, shape fluctuations show up through distortions of the internal structure : indeed the chain ends (ω) are not concentrated near a « centre » of the micelle, and the γ methylene groups do not remain in a spherical shell.

Introduction.

Globular micelles, i.e. aggregates containing approximately 70 amphiphilic molecules each, form spontaneously over a wide range of concentrations in the aqueous solutions of the amphiphile sodium dodecylsulfate (SDS) [1-15]. The structure of such micelles appears to be a matter of chronic concern [16-39] ; indeed, the acquisition of high resolution structural data is a required step for the future design of specific chemical reactions using the micellar surface as a catalyst.

Most of the confusion stems from the following question : should the micelles be pictured as well

(*) This work used the neutron beams of ILL in Grenoble, France.

(+) Laboratoire associé au CNRS.

(++) Current address : DPC/SCM, CEN-Saclay, 91191 Gif-sur-Yvette, France.

defined particles or as a general class of transient, disordered aggregates ? In the first point of view micelles have a highly ordered internal structure; some models select a specific packing of the hydrocarbon chains, such as the parallel/normal packing of Fromherz [35-37] or Menger's earlier « pin-cushion » model [32]; others have a singularity at the centre, such as Dill and Flory's quasi-crystalline order near the centre of the core [28]. If these views are correct, it should indeed be possible to determine a precise structure for the micelle, i.e. a complete set of distances and masses, including a detailed shape for the water/hydrocarbon interface and a specific location for each type of CH_2 or CH_3 group; the fluctuations around the average parameters should be small. In the second point of view, the micelles are better described as liquid droplets of amphiphile if they are large, or as simple fluctuations of the local concentration of amphiphilic molecules if they are small. In this class all the thermodynamic models which consider that surface forces are dominant for micelle formation, and consequently neglect all terms in the free energy associated with the organization of the hydrocarbon chains in a globule [26-22].

This uncertainty can only be resolved by an experiment which measures the amount of order in the internal structure of micelles. For systems with long range order, scattering will give this type of information : the regular packing of the molecules results in a set of diffraction peaks, while various types of disorder will produce either a broadening of the peaks or a diffuse scattering outside the peaks. Here, however, we consider objects in solution; then the scattering is diffuse in every case, i.e. the averages over the positions and orientations of the objects result in a loss of information which precludes such a straightforward separation. Whether an approximate separation can still be performed depends on the system, i.e. on whether the *average structure* of the objects and the *fluctuations away from this structure* can be described with a small set of parameters, and whether the information contained in the scattering curves can determine these parameters without ambiguity. At this point it is appropriate to recall briefly the nature of the information contained in the scattering curves.

2. Methods.

2.1 GENERAL REMARKS. — The scattering pattern can be divided between « small angle scattering » and « wide angle scattering ». *Wide angle scattering* corresponds to distances between neighbouring atoms (1-5 Å); in a liquid there are many such distances which fluctuate and overlap each other. The corresponding interference pattern reduces to a superposition of overlapping diffuse rings which do not yield much useful information. For such distances local techniques such as the NMR measurement of dipolar relaxation rates induced by paramagnetic ions are more appropriate : individual distances can be selected by resolving the chemically distinct nuclei of an amphiphilic molecule [40-42].

Small angle scattering is produced by large scale heterogeneities in the solution (micelles etc. : distances $\sim$ 10 to 1 000 Å, scattering vectors $Q \sim 0.006$ to 0.6 $Å^{-1}$). In this range the molecules can be treated as a continuous medium, and the scattering is controlled by the excess density of scattering length $\rho(\mathbf{R}) - \rho_s$; the scattered amplitude $A(\mathbf{Q})$ is the Fourier transform of $\rho(\mathbf{R})$ in the irradiated volume [43-47]

$$A(\mathbf{Q}) = \int_v (\rho(\mathbf{R}) - \rho_s)\, e^{-i\mathbf{Q}.\mathbf{R}}\, d^3\mathbf{R}. \qquad (1)$$

With respect to the separation between order and fluctuations, the crucial point is that a *static scattering* experiment measures the *flux* of scattered radiation in a given direction, i.e. the *average of the squared amplitude* :

$$I_{stat}(Q) = \langle A(\mathbf{Q}).A^*(\mathbf{Q}) \rangle \qquad (2)$$

where the bracket denotes a thermodynamic average.

For a system made of particles, the scattered amplitude can be decomposed into a sum over the amplitudes scattered by the individual particles :

$$A(\mathbf{Q}) = \sum_i^n A_i(\mathbf{Q})\, e^{-i\mathbf{Q}.\mathbf{R}_i}.$$

Then the scattered intensity contains n single particle terms and n^2 products of amplitudes scattered by different particles [45]

$$I(Q) = \sum_{i=1}^{n} \langle A_i(\mathbf{Q}).A_i^*(\mathbf{Q}) \rangle + \sum_{i=1}^{n} \sum_{j \neq i}^{n} \langle A_i(\mathbf{Q}).A_j^*(\mathbf{Q}).e^{i\mathbf{Q}.(\mathbf{R}_i - \mathbf{R}_j)} \rangle. \qquad (3)$$

If the positions of the particles are not correlated with their orientations nor with their sizes [45-48], then the averages of products corresponding to different particles can be decomposed into products of averages :

$$I(Q) = n \langle |A_i(\mathbf{Q})|^2 \rangle + n^2 \langle A_1(\mathbf{Q}) \rangle^2 \langle e^{i\mathbf{Q}.\mathbf{R}} \rangle \qquad (4)$$

where the last average is taken over all interparticle distances $\mathbf{r} = \mathbf{R}_i - \mathbf{R}_j$ in the solution. These interparticle interferences can be rewritten with the structure factor $S(Q)$ for the centres of mass of the particles :

$$I(Q)/n = \langle |A_1(\mathbf{Q})|^2 \rangle + \langle A_1(\mathbf{Q}) \rangle^2.[S(Q) - 1]. \qquad (5)$$

This formula expresses the central problems for the determination of the structure of a micellar solution. Firstly, the information obtained from the experiment

is limited to an isotropic scattering curve $I(Q)$. Yet 3 functions are required to separate intra- and inter-particle interferences. They are :

— $\langle A_1(\mathbf{Q}) \rangle$: This is the F.T. of the *average radial distribution* of scattering length within one particle.

— $\langle |A_1(\mathbf{Q})|^2 \rangle$: This is the F.T. of the *average distribution of distances* $P(r)$ within one particle; it contains the effects of *non spherical shapes* and *fluctuations in particle size.*

— $S(Q)$: This is the F.T. of the radial distribution function $g(r)$ for the centres of mass of the particles (plus a constant).

Secondly, even if the interparticle interferences can be separated out [12-13], a formidable problem remains for the interpretation of the first term of equation (5). Indeed, there are many choices for the average shape and the distribution of sizes of the micelles which will yield similar forms of $\langle |A(\mathbf{Q})|^2 \rangle$. In particular, Hayter [49] has shown that for any solution of monodisperse ellipsoïds, there is a solution of polydisperse spheres which will yield a similar scattering pattern. In micellar solutions this problem is aggravated because micelles of different shapes will coexist in the solution [54].

2.2 SPATIAL RESOLUTION. — It is instructive to first consider the simpler problem of a solution of particles which are all identical and non interacting. Even in this case the structure of the particles cannot be deduced from the scattering pattern, unless the particles have spherical symmetry [43-47]. Thus, the only tractable approach is to use the most distinctive features of the scattering curves, together with some basic knowledge of the molecules, to build a structural model ; then check whether this model can reproduce the whole scattering curve, and whether it can also explain the properties of the solution ; and, last but not least, consider whether it is unique in this respect.

For this procedure to be meaningful, the number of parameters in the model must be limited to the information content of the scattering curves. This has been discussed on the basis of information theory by Luzzati and Tardieu [50] ; their argument is as follows. Let D_m be the largest dimension of the particles ; then $\langle |A_1(\mathbf{Q})|^2 \rangle$ is the F.T. of a distance distribution function which is zero beyond $r = D_m$. Consequently $\langle |A_1(\mathbf{Q})|^2 \rangle$ is fully defined by an infinite of points spaced by π/D_m. Now the experimental scattering curve only extends to a finite value of Q, say Q_m ; thus only $Q_m D_m/\pi$ of these points are measured (Fig. 1). Typical values for a low-resolution study of micelles are $D_m = 50$ Å and $Q_m = 0.2$ Å^{-1} ; in this case the number of significant points in the scattering curve is $D_m Q_m/\pi = 3$. Thus it would be unreasonable to try to determine more than 3 parameters on the basis of the information content of such a scattering curve. Of course the experiment can measure many more points of the scattering curve in the same Q range (0 to Q_m) ; however this will not improve

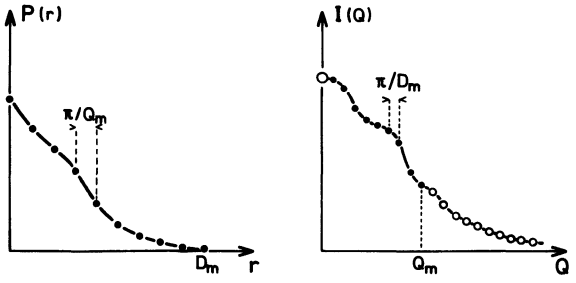

Fig. 1. — Left : distribution of distances $P(r)$ in a hypothetical particule whose largest dimension is D_m ; $P(r)$ is the isotropic average of the Patterson function $P(\mathbf{r})$; it is identical to Porod's characteristic function $\gamma(r)$. Right : the scattering curve for the same particle is fully defined by an infinite set of points spaced by π/D_m ; the experiment measures these values only up to Q_m.

the resolution in r space, unless the data can be safely extrapolated in the region $Q > Q_m$. Without the knowledge of the values of $\langle |A_1(\mathbf{Q})|^2 \rangle$ beyond Q_m, the calculated distribution of distances will be wrong in the region $r = 0$ to $r = \pi/Q_m$; consequently details in the structure corresponding to distances smaller than π/Q_m will not be resolved.

This limitation is illustrated in figure 2, where the distribution of distances $P(r)$ is calculated from intensity curves to which small flat background terms have been added or subtracted, simulating the uncertainty in the background correction. 2 different values of Q_m are used : one typical of a low resolution experiment, and one for high resolution. The truncation of the extra background at Q_m adds an oscillating term to $P(r)$, with a period π/Q_m. The nodes of each set of $P(r)$ curves are the $Q_m D_m/\pi$ points which are truly determined by the experiment, regardless of the accuracy with which $I(Q)$ goes to zero beyond Q_m ; their spacing defines the resolution of the experiment. Remark that this method provides a criterion for determining the correct value of the background correction ; this criterion is more general than the extrapolation of $I(Q)$ according to Porod's law, especially in the case where the available Q range for the Porod regime is too small.

Surprisingly, it has sometimes been claimed that details finer than the resolution can be resolved through contrast variation. Through an appropriate labelling of the polar heads, it may be possible to measure selectively either the *average* radius R_c for the hydrocarbon core of a micelle, or that for the whole micelle, core plus polar layer, R_p [51]. These radii can be measured very precisely even with a small Q range, because they only depend on the values of $\langle |A_1(\mathbf{Q})|^2 \rangle$ near $Q = 0$, or rather the values of its F.T. near D_m. Yet the average thickness σ of the polar layer cannot be deduced from such experiments ; it is not equal to $R_p - R_c$, as can be seen from building

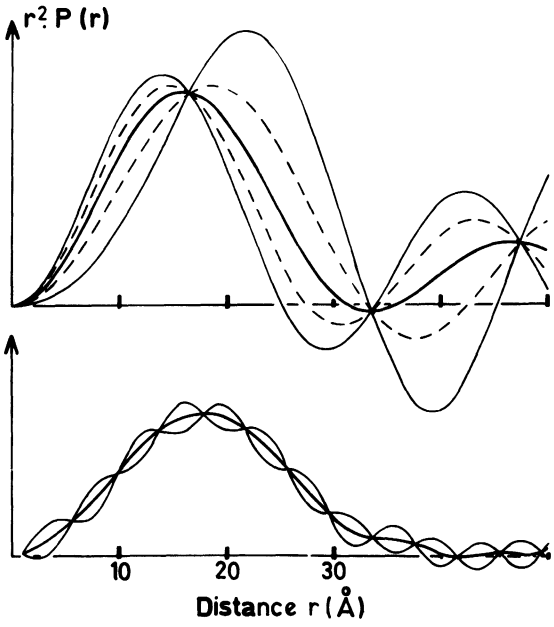

Fig. 2. — Effect of uncertainties in the high Q tail of the scattering curves. The data only extend to Q_m; for this reason the exact baseline is not known accurately, and various background corrections are attempted. The resulting curves are Fourier transformed to yield the distribution of distances in the scattering particles; the oscillations in these distributions are produced by the truncation at Q_m of the background correction; the correct background is the one which produces no oscillations. The nodes of the oscillation pattern are the only points in $P(r)$ which are determined without ambiguity, regardless of the background correction; their spacing is equal to the theoretical resolution π/Q_m. Top : scattering by a sphere of radius 20 Å, truncation at Q_m = 0.24 Å^{-1}. Bottom : same but Q_m = 1 Å^{-1}.

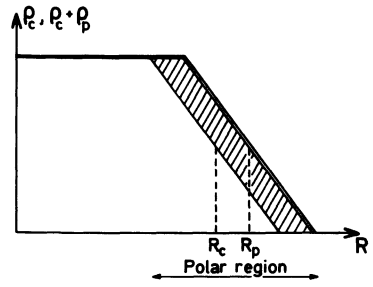

Fig. 3. — Radial profiles of scattering density for the core ρ_c and for the core + polar layer $\rho_c + \rho_p$, of a hypothetical micelle. A low resolution scattering experiment will measure the radii R_c and R_p, but will not give any information concerning the thickness of the polar layer.

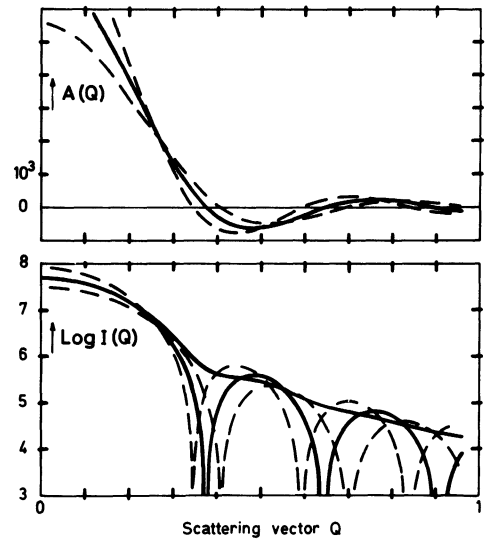

Fig. 4. — Top : amplitude scattered by a micelle for a given orientations of the micelle and of the scattering vector Q; the dotted lines correspond to various fluctuations in orientation, shape and size of the micelle, and the full line to the thermodynamic average. Bottom : scattered intensities; the effect of fluctuations is negligible at small Q, and dominant at large Q where the individual scattering curves are out of phase.

models with interfacial layers of various thickness (Fig. 3). In fact, this thickness can only be obtained from experiments at Q values approaching π/σ. Similar arguments apply for micelles with an irregular surface [52].

2.3 EFFECTS OF FLUCTUATIONS OF SIZE AND SHAPE. — Even if a good resolution could be attained for the distances in a solution of *identical* particles, with micelles their fluctuations in size and shape will limit the analysis of the data taken at high resolution. Consider first the *amplitude* $A(\mathbf{Q})$ scattered by a micelle of given orientation : this is an oscillating function with zeros at regularly spaced values of $\mathbf{Q}$. Size and shape fluctuations, as well as the reorientations of the micelles will shift the positions of these zeros (Fig. 4a). These effects are averaged out in the thermal average $\langle A_1(Q) \rangle$, which is an oscillating function of the same type; similarly, the average of the squared amplitude will retain the same zeros. However the individual *intensities* $\langle | A_1(\mathbf{Q}) |^2 \rangle$ will only show weak minima instead of zeros (Fig. 4b).

This effect of size and shape fluctuations is largest at high values of Q where the individual amplitudes corresponding to each fluctuation are out of phase; it is negligible at low Q where they are all in phase. Consequently a low resolution picture for the average micelle can be extracted from the low Q part of the scattering curves, whithout having to worry about the fluctuations in size and shape. Problems will occur for the analysis of high Q data, where high resolution details of the average structure and effects of the fluctuations are both important.

2.4 CONTRASTS. — After all these warnings, we must emphasize that neutron scattering from micellar solutions has one bright side; that is the manipulation of contrasts through isotopic substitution [43, 10-15].

Indeed, the density $\rho(\mathbf{R})$ which controls the scattering is a sum over the scattering lengths b_i of all nuclei in a volume which is larger than interatomic distances but small compared to the resolution of the experiment :

$$\rho(\mathbf{R}) = n_1(\mathbf{R}).b_1 + n_2(\mathbf{R}).b_2 + \cdots \quad (6)$$

Through isotopic substitution the scattering lengths b_i can be modified without changing the structure, and therefore the set $n_i(R)$; thus additional relations concerning this structure can be derived. The main isotopic substitution is that of H by D; this will shift the scattering length of methylene groups from one end of the range of scattering lengths to the other (Table I). In the present work we have used molecules of the surfactant sodium dodecyl sulfate (SDS) which have been labelled in 4 different ways :

$C_{12}H_{25}SO_4Na$ (fully protonated, or « p_{25} »)
$C_{12}D_{25}SO_4Na$ (fully deuterated, or « d_{25} »)
$(CD_3)(C_{11}H_{22})SO_4Na$ (methyl deuterated, or « $12d_3$ »)
$(C_9H_{19})(CD_2)(C_2H_4)SO_4Na$ (γ deuterated, or « $3d_2$ »).

By using either H_2O or D_2O as a solvent for these molecules, we generate 8 micellar solutions, each corresponding to a different contrast of the methylene groups against the solvent, but all sharing the same structure, provided that such isotopic substitutions do not perturb the micelle.

Comparing the scattering from SDS-$12d_3$ with that from SDS-p_{25} in the same solvent will provide some information on the distribution of the end groups in a micelle. Specifically, what is measured through this comparison is not the distribution of positions $n(\mathbf{R})$ but the distribution of distances $P(r)$ between CD_3 groups, under some assumptions which are discussed in § 6.1. Similarly, the distribution of distances between γ methylene groups can be calculated by comparing SDS-$3d_2$ with SDS-p_{25}. Finally, the distribution of distances for the whole core should in principle be calculated by comparing SDS-p_{25} with SDS-d_{25}; for this case, however, it is sufficient to use a single spectrum taken at high contrast, either p_{25} in D_2O or d_{25} in H_2O, since the spectra taken at low contrast, either p_{25} in H_2O or d_{25} in D_2O, contain much less intensity (Appendix 1).

Table I. — *Volumes and scattering densities.*

Chemical group	b	v	v_0	ρ
CH_2	− 0.083	16.24	27	− 0.308
CH_3	− 0.457	32.7	54.3	− 0.841
CD_2	1.999	16.24	27	7.41
CD_3	2.666	32.7	54.3	4.91
SO_4Na	2.965	40.82	67.8	4.37
$C_{12}H_{25}$	− 1.37	212.94	353.7	− 0.387
$C_{12}D_{25}$	24.655	212.94	353.7	6.97
$C_{12}H_{25}SO_4Na$	1.595	246.82	410	0.389
$C_{12}D_{25}SO_4Na$	27.62	246.82	410	6.736
H_2O	− 0.168	18.1	30	− 0.56
D_2O	1.92	18.1	30	6.39

b = Scattering length per group in cm × 10^{12}
v = molar volume, in cc/mole, from Luzzati *et al.* at 24 °C [8, 9]
v_0 = volume per group in Å^3 at 24 °C
ρ = $b \times N_{av}/v$ = density of scattering length in cm^{-2} × 10^{10} or in Å^{-2} × 10^{-6}.

Without these labelling experiments, the scattering information on micellar structures would remain largely ambiguous, because the average over all fluctuations would make it impossible to decide between different high resolution models. However, in all such structural models, the distributions of distances $P_{CD_3}(r)$, $P_{CD_2}(r)$, and $P_{core}(r)$ are interdependent, because the micelle is made of SDS molecules rather than of independent CD_3, CD_2, and SO_4Na groups. Most of the structural models which could fit one of these 3 distributions will not fit them together when this constraint is taken into account; this eliminates a substantial part of the ambiguity in structure determination.

All these procedures rely on the measurement of complete scattering curves, allowing the distributions of distances to be calculated through a Fourier transform. In the past, there have been claims that the penetration of water molecules in the micelle could also be assessed from the $Q \to 0$ limit of the scattered intensity, through a substitution of H_2O by D_2O or of p_{25} by d_{25} [14, 15, 31]. The argument was that the composition of the « wet » micelle could be determined by measuring the variations of the average scattering density $\bar{\rho}$ of the micelle in such substitutions. However the small angle scattering is only produced by the *excess* scattering density $\rho(\mathbf{R}) - \rho_s$ of the micelles with respect to water, as expressed in equation (1); if water molecules are included in the micelle, they will contribute equally to the terms $\bar{\rho}V$ and $\rho_s V$ of the integral at $Q \to 0$; consequently their net effect on the intensity will be zero [60].

This last problem can easily be solved by considering those distances which are seen through small angle scattering, that is $P_{core}(r)$. Indeed, for a given aggregation number N of the micelle, the penetration of water molecules would swell the core, and consequently expand the spatial range of $P_{core}(r)$. Since both N and $P_{core}(r)$ are measured with a very good accuracy, a precise upper limit can be set for the amount of water which may swell the core (§ 5.2).

2.5 OUTLINE. — As indicated in § 2.2, the information content of the scattering curves is directly proportional to the range of scattering vectors covered by the experiment. In the present work, 3 different experiments have been combined to obtain a Q range as large as allowed by the conditions of small angle scattering; the way in which these data have been obtained and treated is described in section 3.

Next, the low Q part of the scattering curves is used to obtain a low resolution picture for the *average*

structure of the micellar solution (Sect. 4). In this range of Q vectors the correlations between different micelles have very large effects; they are described according to the method of Hayter and Penfold [12]; the average aggregation number $\overline{N}$ and charge $\overline{Z}$ of a micelle are obtained *via* this procedure.

In section 5, the whole scattering curve of SDS-p_{25} in D_2O is used to obtain a high resolution picture for the hydrocarbon core of a micelle. This scattering curve shows damped oscillations superimposed on an asymptotic Q^{-4} law. As explained in § 2.3, the oscillations are controlled by the detailed average shape *and* by fluctuations in size and shape. The asymptotic behaviour is related to the structure of the water/hydrocarbon interface.

Finally, the scattering curves of labelled micelles are used in section 6 to determine how specific methylene or methyl groups are distributed within the hydrocarbon core of a micelle. Again, a high resolution picture requires the use of a Q range where the effects of fluctuations in size and shape must be taken into account. This can be done by comparing the average distribution of distances for labelled groups with that for the whole hydrocarbon core.

3. Scattering experiments.

Scattered intensities are collected according to the magnitude of the scattering vector $\mathbf{Q}$, where $Q = (4\pi \sin\theta)/\lambda$, 2θ is the scattering angle, and λ the wavelength of incident neutrons. Energy transfers to and from the neutrons during scattering are ignored according to the static approximation; this justifies the use of equation (2), where both $A(\mathbf{Q})$ and $A^*(\mathbf{Q})$ refer to the same time in the sample [47].

The range of Q values is $0.015 < Q < 1$ Å^{-1}. These values cover the whole range of distances relevant to the micellar solutions, with the lower Q values corresponding to dimensions much larger than intermicellar distances, and the higher ones to distances much smaller than the micellar diameter. At high Q the small angle scattering caused by the micelles becomes very weak, and wide angle scattering sets in; indeed, water has a very broad peak around $Q = 2$ Å^{-1}, and the distances between neighboring SDS chains also produce a diffuse band centred at 1.4 Å^{-1}. Consequently, the scattering from the solutions, after dropping by a factor of 10^4 from 0.06 to 0.6 Å^{-1}, begins to rise again beyond $Q = 0.7$ Å^{-1}. We choose this value as the crossover from small angle to wide angle scattering. Data obtained between 0.7 and 1 Å^{-1} were used only for the purpose of refining the background subtraction.

A first set of experiments was performed by combining the spectrometers D11, D17 and D1B of ILL; two years later, an independent set of spectra was obtained with 4 detector positions of D16.

D11 : $0.015 < Q < 0.09$ Å^{-1}	$\lambda = 6$ Å	$\Delta\lambda/\lambda = 8\%$ FWHM
D17 : $0.022 < Q < 0.13$	$\lambda = 10$	$\Delta\lambda/\lambda = 10\%$
D1B : $0.1 < Q < 1$	$\lambda = 2.5$	$\Delta\lambda/\lambda = 1\%$
D16 : $0.02 < Q < 0.8$	$\lambda = 4.5$	$\Delta\lambda/\lambda = 1.5\%$.

For each detector position, the collimation was adjusted so that the $\Delta Q/Q$ resulting from the divergence of the beam was less than 10 % (55). Multiple coherent.coherent scattering was negligible, as evidenced by the ratios of sample transmission to blank transmission, which were always above 0.98. The data from each instrument were treated according to standard ILL procedures for small angle scattering : radial averaging, correction for attenuation of the beam and normalization of the efficiency of the detector cells by H_2O($Q < 0.7$ Å^{-1}) or vanadium (for D1B) [56]. Once normalized, the data from D11 and D17 fell within 5 % of each other, those of D17 and D1B within 10 %; a final adjustment then yielded a single scattering curve for the whole range of Q. For D16, the data from different detector positions fall within 2 % of each other after normalization by H_2O.

At large Q the sample spectra are matched by the blanks within 10^{-3} of the peak intensity. The residual differences cannot be controlled because of uncertainties in the relative transmissions of samples and blanks (D16) or in counting the flux of incident neutrons (D1B). This problem can be handled by assuming that the small angle scattering caused by the structures of the particles must go to zero at large Q. For large particles, Luzzati and Tardieu [50] assume that the sample spectrum behaves asymptotically as $AQ^{-4} + B$. Then a plot of IQ^4 *vs.* Q^4 yields the Porod limit A and the residual background B. However for micelles the scattering at large Q oscillates around this law, making the extrapolation difficult. Alternatively, the data can be Fourier transformed to obtain the distribution of distances $P(r)$. As shown in figure 2, an incorrect subtraction of background adds a flat term truncated at Q_{max}, resulting in oscillations with a period π/Q_{max} in $P(r)$. The correct background subtraction is then obtained by minimizing these oscillations.

At low Q the data were treated directly trough the ILL programs developed by J. B. Hayter to extract the intermicellar interferences. Then it was necessary to extrapolate the single particle scattering to $Q \to 0$;

otherwise a gap around $Q = 0$ would produce a negative correlation at large r in the distribution of distances $P(r)$.

Some treatments involved the comparison of spectra obtained with 2 types of labelling. For this purpose the precision on absolute intensities was insufficient, and it was necessary to rescale these intensities according to the theoretical densities of scattering length. Finally, it was also necessary to remove one weak specular reflexion observed on one position of D16.

4. Low resolution structure of the micellar solution.

The scattering curves of 2 % SDS solutions show a prominent peak at low Q vectors, which depends on the concentration of micelles. Moreover, similar peaks are observed in the scattering curves of other charged particles in water. As shown by Hayter and Penfold [12], those peaks are produced by interferences of neutrons scattered by nuclei located on *different* particles. Such interparticle interferences would be averaged out if the particles were able to take completely random positions in the solution, as in a perfect gas. However, when the particles repel each other, especially through long range electrostatic potentials, their positions become correlated, and these correlations yield a non trivial factor in the expression of the scattered intensity. A mathematical expression of these statements lies in the general expression for the scattered intensity, equation (5). In this expression the interparticle interferences are expressed by the structure factor $S(Q)$. At low values of Q, corresponding to distances much larger than the average intermicellar distance, $S(Q)$ becomes equal to the osmotic compressibility of the micellar solution, which is quite low-thereby depressing the scattered intensity. Then for Q values which are comparable but not equal to the average *inter*micellar distance, $S(Q)$ shows the well known peak. Finally, for Q values corresponding to *intra*micellar distances, $S(Q)$ approaches 1, and the scattered intensity is dominated by the first term of equation (5). The classic problem in the scattering of micellar solutions is the separation of such interparticle interferences from the intraparticle terms which correspond to the structures of the micelles [45-49].

An analytic form of $S(Q)$ for charged particles in water has been found by Hayter and Penfold [57]; at low particle concentrations the rescaled mean spherical approximation of Hansen and Hayter [58] must be used. A structure factor $S(Q)$ calculated according to this model can be extracted from the measured intensity $I(Q)$ through a self consistent fitting procedure [12, 13]. Figure 5 presents the resulting decomposition of $I(Q)$ for our SDS solutions.

The steps followed in the use of this procedure are as follows [52]. An approximate model for the structure of the micelle is chosen, with 2 adjustable parameters : the average aggregation number $\overline{N}$ and the average charge $\overline{Z}$. We ignored the effects of fluctuations in shape, size and charge of the micelles, and therefore the differences between $\langle | A_1(\mathbf{Q}) |^2 \rangle$ and $\langle | A_1(\mathbf{Q}) | \rangle^2$. This is justified because such differences are small at low Q (§ 2.3). The program then calculates $\langle | A_1(\mathbf{Q}) | \rangle^2$ and $S(\mathbf{Q})$ with an initial choice of the average parameters, and compares the resulting theoretical curve with the experimental one; then the values of $\overline{N}$ and $\overline{Z}$ are corrected and the procedure is iterated.

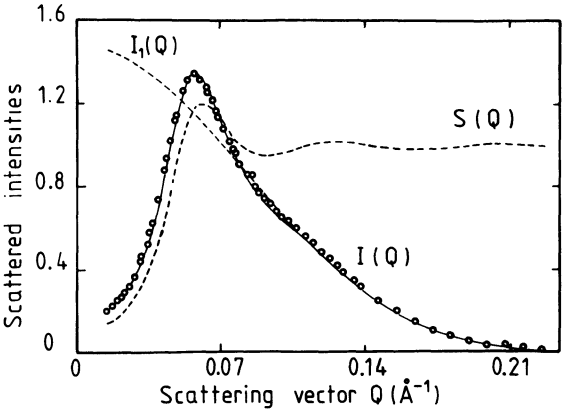

Fig. 5. — Scattering data from a 2 % solution of SDS in S_2O. The dashed lines are the intermicellar structure factor and the single micelle scattering function $I_1(Q) = \langle | A_1(\mathbf{Q}) |^2 \rangle$ calculated through the procedure of Hayter and Penfold; the resulting fit to the data is indicated as a full line.

For SDS-p_{25} in D_2O at a concentration $C =$ 0.02 g/cc and with no added salt, the best fit is obtained for $\overline{N} = 73.6$ and $\overline{Z} = 28$. For SDS-d_{25} in H_2O, $\overline{N} = 68.1$ and $\overline{Z} = 24$. From these values the effect of deuteration on the aggregation of pure SDS appears to be small [67].

It is important to note that such values of $\overline{N}$ are derived essentially from the peak's position — by measuring intermicellar distances and micellar sizes, not from the absolute magnitude of the intensities. Indeed, only the shape and position of the experimental peak in $I(Q)$ are used as criteria for the fit, not its absolute magnitude. Therefore, the comparison of the respective scales for calculated and experimental intensities can be used to check whether the model is meaningful. For this comparison, the experimental intensities must be measured on an absolute scale. This can be done in 2 ways. Either the measured intensities are normalized by the incoherent scattering of H_2O; the uncertainty on the resulting scale is $\pm$ 20 %, due to inelastic effects in the scattering of H_2O. Or, they can be divided by the integral of scattered intensities in reciprocal space, i.e. Porod's invariant (Appendix 1); the precision on this result is very good if the whole Q range is covered. Table II shows the corresponding values of the aggregation number $\overline{N}$.

For dilute solutions of SDS at high contrast, where the hydrocarbon core of the micelle dominates its scattering, all 3 ways of measuring $\overline{N}$ are in good

Table II. — *Average aggregation number of SDS micelles.*

Sample	(a)	(b)	(c)	Average
SDS-p_{25} in D_2O	73.6*	67*	70.5×	75.3
	79+	79+	83+	
SDS-d_{25} in H_2O	68.1*	60.6*	61.4×	63.4
SDS-12 d_3 in D_2O	83.7+	74+	105.4+	
			76.4×	84.9
SDS-3 d_2 in D_2O	78.4+	58.4+	93+	79.6
			88.7×	
Average	78.6	67.8	82.6	76.5

(a) From the position and shape of the peak in $I(Q)$, according to the procedure of Hayter and Penfold [12].

(b) From the $Q \to 0$ limit of the single particle scattering, normalized by the scattering of H_2O.

(c) Same as (b), but normalized by Porod's invariant $\int_0^{Q_{max}} Q^2 I(Q)\, dQ$.

* Data from D17.

\+ From D16.

× From D1B.

agreement. Thus the fitting procedure has produced a meaningful separation of intermicellar and intramicellar interferences. Furthermore, this separation does not depend on the details of the models which describe micellar structures and interactions between micelles : indeed we find that slight variations in the structural model, such as changes in the relative compositions of the 2 shells, or in the hydration of the micelle, result in identical fits to the scattering curves within the Q range of figure 5. This is to be expected, since the separation applies to distances comparable to intermicellar distances in the solution ($d \sim 100$ Å) whereas the details of micellar structure correspond to much smaller distances. It is only for much higher surfactant concentrations ($\phi \sim 0.5$) that the details of micellar structure will affect the intermicellar interactions [59].

At low contrast, the core and the polar layer give comparable contributions to the scattered amplitudes; the resulting scattering curve for a single micelle can be altered drastically by small changes in the volumes assigned to various groups or in the hydration of the polar layer, even at the 15 Å resolution level. Then the same thermodynamic model with the same values of $\overline{N}$ and $\overline{Z}$ still provides a reasonable separation of intermicellar and intramicellar interferences; however the absolute intensity scales are no longer predicted accurately, presumably because of errors in the values of the scattering densities [52]. High resolution data at low hydrocarbon/water contrast would be needed to obtain a model for the polar layer; for this problem X ray scattering is clearly more appropriate than neutron scattering [63].

5. Size, shape and fluctuations.

Beyond the intermicellar peak shown in figure 5, the scattering curves show *damped oscillations* superimposed on a Q^{-4} asymptotic law. This high Q tail can be used to obtain a high resolution picture of a micelle. In this section we consider data taken at high contrast between the hydrocarbon core and the solvent, specifically SDS-p_{25} in D_2O. Then the scattering is effectively controlled by the core (see Appendix 1); the damped oscillations depend on its average size, average shape, and fluctuations, while the asymptotic decay relates to the structure of the hydrocarbon/water interface.

5.1 SIZE AND SHAPE. — All objects of simple geometry produce characteristic oscillations in the high Q tail of the scattered intensity. As such oscillations are superimposed on a fast asymptotic decrease of the intensity, they cannot be seen in a plot of $I(Q)$ *vs.* Q such as figure 5. The asymptotic law is often close to Q^{-4}; then the best representation for the pattern of oscillations is a plot of IQ^4 *vs.* Q. Figure 6 shows this type of plot for SDS-p_{25} in D_2O together with the theoretical curves for polydisperse homogeneous spheres.

At this point it is appropriate to define which parameters remain fixed for all models and which ones are adjusted. There is one quantity which is determined by the experiment with very good precision : it is the average aggregation number $\overline{N}$. We take $\overline{N} = 74$, which yields a *hydrocarbon* volume of 25 914 Å^3. Note that this is a « dry » volume, excluding all water which might have penetrated into the micelle. Indeed the aggregation number $\overline{N}$ is calculated by counting the number of micelles in the solution, and does not

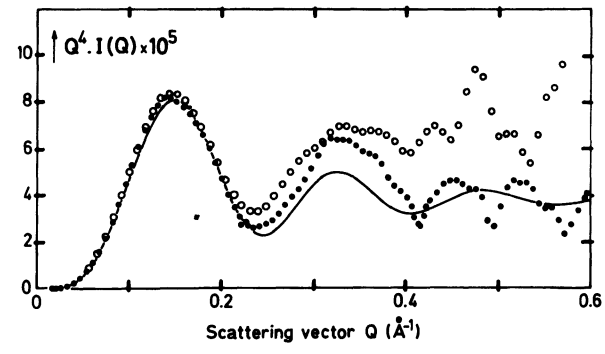

Fig. 6. — High Q data for SDS-p_{25} micelles in D_2O. For compact spheroidal particles, the scattering curves always oscillate around a Q^{-4} asymptotic behaviour; the oscillation pattern is damped by the polydispersity of the sizes and by deviations from the spherical shape; it is best revealed by a plot of $Q^4 I(Q)$ *vs.* Q as shown here. Dots : single particle scattering obtained from D16 data and normalized to $I(Q \to 0) = 1$. Circles : same from D1B data. Full line : calculated for a polydisperse distribution of homogeneous spheres; their average volume matches the measured aggregation number of SDS micelles.

depend on micellar hydration. This number sets the intensity scale for the single micelle scattering in all models, again regardless of hydration : indeed any water which might have penetrated in the micelle or be associated with it does not contribute to $\langle | A_1(Q \to 0) |^2 \rangle$; previous assertions to the contrary [14, 15, 31] are in error (see § 2.4 and Ref. [60]). Consequently all models where the average hydrocarbon volume per micelle is equal to 25 914 Å^3 will fit the $Q \to 0$ limit of the single micelle scattering; the intensity scales of these scattering curves can no longer be adjusted to improve the fit in another range of Q. At this point the parameters which do remain free are the distribution of micellar aggregation numbers (or volumes) and the micellar shapes.

For any solution where micelles of various aggregation numbers are in equilibrium with each other as well as with free DS^- ions, the width of the distribution in N can be estimated from the variation of $\overline{N}$ with the concentration x_m of micellized SDS through a general thermodynamic relation [21] :

$$\frac{\sigma^2}{\overline{N}^2} = \frac{\partial \operatorname{Ln} \overline{N}}{\partial \operatorname{Ln} x_m}.$$

This variation has been measured by Hayter and Penfold [13], as well as by previous light scattering experiments [1-6]. Accordingly, in a 2 % solution of SDS, this polydispersity should amount to :

$$\sigma_N/\overline{N} = 0.33 \quad \text{or} \quad \sigma_N^2/\overline{N}^2 = 0.1 .$$

Thus, the weight averaged aggregation number is 82, while the number average is of course 74. Remark that the corresponding distribution of radii has a much smaller width :

$$\sigma_R/\overline{R} = 0.1 \quad \text{or} \quad \sigma_R^2/\overline{R}^2 = 0.01 .$$

A direct confirmation of this estimate is provided by the electron microscope observations of Bachmann, Dasch and Kutter [64] : for amphiphiles with slightly longer alkyl chains the standard deviation of the radii is also found to be one tenth of the average radius.

On the other hand the choice of the distribution of sizes is not imposed *a priori*. Many different distributions have been used by other authors [46, 48, 49] and at low resolution it is usually assumed that they yield equivalent results. This is not the case at high resolution; in particular, the asymptotic limit of $I(Q)$ is dominated by the smallest micelles, which contribute very little to the $Q \to 0$ limit. In the present work we take a Gaussian distribution of the aggregation numbers.

Finally, for the sake of simplicity, we assume that all micelles share the same shape, i.e. shape fluctuations are neglected, although in reality they must be comparable to size fluctuations [53, 54]. Then the only parameters which remain free for the fit are the choice of the average shape, and the average anisotropy of this shape. We now examine the fits obtained with the various shapes.

Spheres. The fit by a distribution of homogeneous spheres with an average radius $R = 18.4$ Å is shown in figure 6, solid line. The distribution of their volumes is Gaussian with a half width of 40 % corresponding to a standard deviation $\sigma^2/\overline{N}^2 = 0.16$. In this representation the height of the first maximum at $Q = 0.15$ Å^{-1} is controlled by the average diameter of the particles; here the theoretical curve is within 10 % of the absolute intensity measured by the experiment. At $Q = 0.24$ Å^{-1} the curves reach the first minimum, which is controlled by the polydispersity of the volumes; the agreement at this point indicates that the value chosen for their standard deviation is reasonable. Finally, the rest of the oscillating pattern is properly matched, and the asymptotic limit of the fit is comparable to that of the data; this last point indicates that the distribution of the volumes contains an appropriate fraction of small spheres.

We conclude that the general pattern of oscillations shown by the data is reproduced by homogeneous spheres; however a slight mismatch appears around the second maximum of the IQ^4 plot, presumably caused by deviations from spherical shape.

Ellipsoids. Figure 7 shows the fits obtained with either prolate or oblate ellipsoids; it is assumed that these ellipsoids are homogeneous, polydisperse in size but not in shape, and take random orientations; their average volume is fixed and equal to that of a 18.4 Å sphere. For axial ratios below 1.3, the general pattern of oscillations is reproduced, but the curves are almost undistinguishable from those for polydisperse spheres. For larger axial ratios the height of the first maximum is reproduced, but the pattern of oscillations has the wrong period. Clearly, no choice of axial ratio will give a satisfactory fit to the data once the average (or $\overline{N}$) has been fixed.

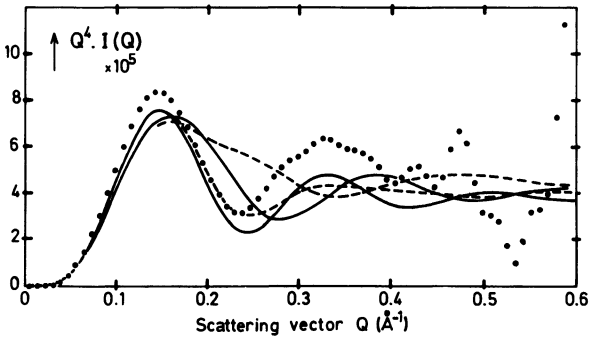

Fig. 7. — The data from D1B are fitted by the theoretical curves for ellipsoids whose volumes match the average aggregation number of SDS micelles. The 2 solid lines correspond to prolate ellipsoids with axial ratios $e = 1.3$ (shorter period) and $e = 2$ (longer period). The dashed lines are for oblate ellipsoids with axial ratios $e = 0.7$ (shorter period) and $e = 0.5$ (loss of the minimum).

Cubes. Fromherz has proposed that micelles may be built of surfactant blocks assembled at right angles [35-37]. In his model disorder is introduced through vacancies and dislocations; the resulting shape may then be indistinguishable from a sphere. It is nevertheless interesting to see whether the original object, a cuboid, can be distinguished from a sphere. Figure 8 shows the calculated curves for monodisperse homogeneous cuboids and for polydisperse cubes; the average volume per object is fixed as before. Such objects fail to reproduce the observed scattering because their flat surfaces produce exagerated oscillations.

Irregular shapes. A class of spheroidal particles with pseudo-irregular surfaces can be generated by introducing large cavities in the outer layer of homogeneous spheres. Spherical cavities allow the scattering to be calculated analytically; this choice is of course quite arbitrary, but at the present scale of resolution different types of cavities would yield identical results. The anisometry of the particles and the scale of the irregularities are then controlled by choosing the number of cavities and their radii. Figure 9 shows the

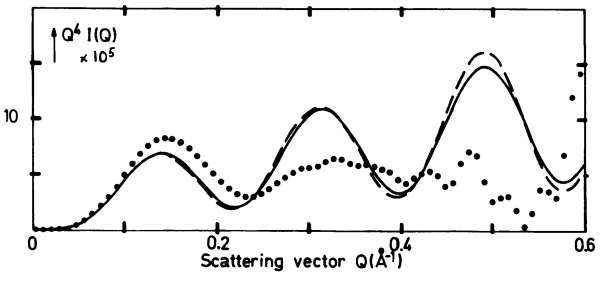

Fig. 8. — Fits by cuboids. Full line : monodisperse cuboids with edges 26.64, 29.6, and 32.89 Å. Dotted line : polydisperse cubes, $\frac{\sigma}{N}$ = 40 %, average edge 29.6 Å.

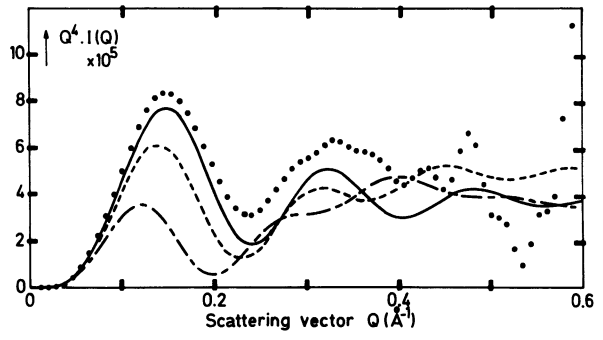

Fig. 9. — Fits by spheres with cavities. ---- : sphere of outer radius R = 19.4 Å, with 6 cavities of radius 5.5 Å located in the outer layer of the main sphere. The filled volume matches the average aggregation number of a SDS micelle, while the cavities contain 2 water molecules per SDS molecule. - — - : same with 8 water molecules per SDS molecule in the cavities. ——— : full sphere.

curve calculated with 6 spherical cavities located with cubic symmetry in the outer layer of a sphere; the total volume of the cavities has been chosen to match the known hydration number of the SDS micelle, and the radius of the sphere is adjusted to keep the volume of the particule identical with that of an homogeneous 18.4 Å sphere. Obviously the inclusion of cavities at constant hydrocarbon volume swells the core; consequently the intensity decreases faster with Q, and in the IQ^4 plot the first maximum is too low, even if the cavities only contain 2 water molecules per SDS molecule. The smallest amount of water inside the core which could not be detected in this way must be less than one water molecule per SDS molecule.

Conclusions on the shape. The experimental scattering curves obtained at high contrast set 3 constraints for the size and shape of SDS micelles. Firstly, the low Q range of scattering measures the aggregation number $\overline{N}$ in 2 different ways; we find $\overline{N}$ = 74, which yields an average volume of hydrocarbon equal to that of an 18.4 Å sphere. Secondly, the oscillation pattern observed between Q = 0.1 and 0.4 $Å^{-1}$ corresponds to a spherical shape with the same radius. Thirdly, the oscillations are strongly damped; this damping cannot be explained by a deviation of the *average* structure away from the spherical shape; however it can be matched by letting the sizes of the spheres fluctuate around their average value; these fluctuations are large but comparable to thermodynamic predictions for SDS.

Although non spherical shapes are ruled out for the average structure, they should be allowed in the fluctuations away from the average. Indeed, the general descriptions of such fluctuations [53, 54] are based on a series of even-order spherical harmonics including l = 0 (monopole) and l = 2 (quadrupole) [44]. However the problem is complicated by the constraints of molecular packing, which may couple different harmonics to each other. Indeed, the fits by ellipsoids shown in figure 7 indicate that fluctuations of anisotropy at constant volume will not fit the data; a better agreement would probably be obtained with fluctuations which leave one dimension of the micelle unchanged.

5.2 WATER/HYDROCARBON INTERFACE. — One problem of current interest is the structure of water/hydrocarbon interfaces : is water/hydrocarbon contact limited to a thin layer, or is there substantial water penetration between the aliphatic chains of surfactant molecules ? This problem involves the measurement of short distances, which are reflected in the high Q region of the scattering curves. For example, sharp interfaces will yield scattering curves which follow Porod's law, $I(Q) \propto Q^{-4}$ (see Refs. [43-45, 47]). Diffuse boundaries will produce a scattering which drops much faster than Q^{-4} at large Q. In the case where the interface is a step function smoothed by a Gaussian

of width e, the asymptotic trend is :

$$KI(Q) \simeq 2\,K(\bar{\rho} - \rho_s)^2\, SQ^{-4} \exp(-e^2 Q^2). \quad (7)$$

The main problem in trying to compare the experimental data with these asymptotic laws is the accuracy of the background subtraction. This problem can be solved when the structure-related scattering follows a simple law in Q; then the measured intensity can be plotted in a way which does not depend on the accuracy of the background subtraction. For example, the intensity obtained with an approximate subtraction of a background can be plotted as $I(Q)$ *vs.* Q^{-4}. If the structural term follows Porod's law, the total intensity will be of the form :

$$I(Q) = AQ^{-4} + B \quad (8)$$

where B is the residual background and A the average surface area per particle.

Figure 10 shows this type of plot for the data obtained on DIB; here the data at low Q have been left out (beyond the right hand side of the figure); they are followed by the distinctive oscillations of spherical particles, and then by the asymptotic range at the left hand side. The asymptotic behaviour follows Porod's law.

A good fit to the data is obtained with the theoretical curve for spheres with sharp boundaries (curve 1), provided that the average volume and polydispersity of these spheres are set as explained in § 5.2.

Curve 2 shows an attempt to fit the data according to equation (10), assuming that the spheres have diffuse boundaries with a thickness comparable to the resolution of the experiment : the full width at half maximum (FWHM) of the broadening function in equation (10) is $2e = 4$ Å. Although the fit is acceptable at low Q (large values of Q^{-4}, beyond the right hand edge of the figure), it fails in the asymptotic range where the predicted intensities are too small by a factor of 2.

A similar result is obtained with « staircase » boundaries, where the density of hydrocarbon falls in 5 sharp steps spaced by 2 Å each : here as well the FWHM of the boundary layer is 4 Å, and the densities have been adjusted so that the overall content is identical with that of the 18.4 Å sphere. This curve is compared in figure 11 with the data from D16 : again the diffuse boundary is ruled out by the data.

Thus any model where *isolated* water molecules would penetrate substantially in between the hydrocarbon chains yields an intensity which drops much faster at high Q than observed asymptotic behaviour. On the other hand, it has been shown in the preceding section that interfacial layers with *larger irregularities* such as cavities will produce a scattering which remains higher than the data in the asymptotic range (Fig. 9). Therefore one might wonder whether a fortuitous combination of these effects might not reproduce the observed asymptotic law. Figure 12 shows that such a compensation is indeed possible at high Q; however at low Q both effects (isolated water molecules and cavities) work in the same direction and produce an increase in the largest diameter of the micelle; as a result the first maximum of the IQ^4 plot is no longer reproduced.

We conclude that, on a scale comparable with the resolution of the experiment, i.e. 5 Å, the SDS micelles have sharp water/hydrocarbon boundaries; the overall penetration of water into the hydrocarbon core must be no more than one water molecule per SDS molecule.

6. Internal organization of the core.

6.1 METHOD. — In regular SDS micelles (SDS-p_{25}), all the chemical groups of the core have similar scattering densities (Table I); in small angle scattering

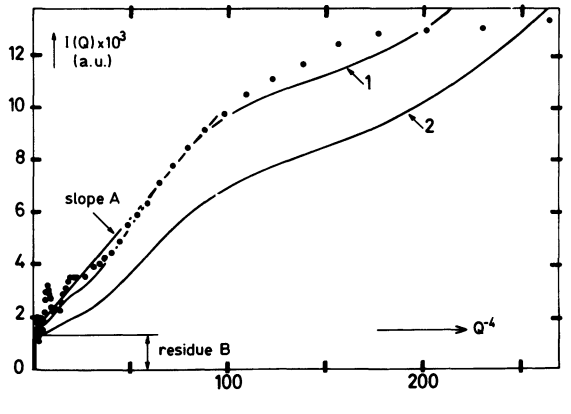

Fig. 10. — Asymptotic trend at high Q for SDS-p_{25} in D_2O; surfactant concentration 2 %, no added salt. The values of Q range from 0.24 Å^{-1} at the right hand side of the figure to 1 Å^{-1} at the left hand side. The intensities are unsmoothed data in absolute units. The straight line is a fit to Porod's law; line 1 is a fit by spheres with sharp boundaries, and line 2 by spheres with diffuse boundaries.

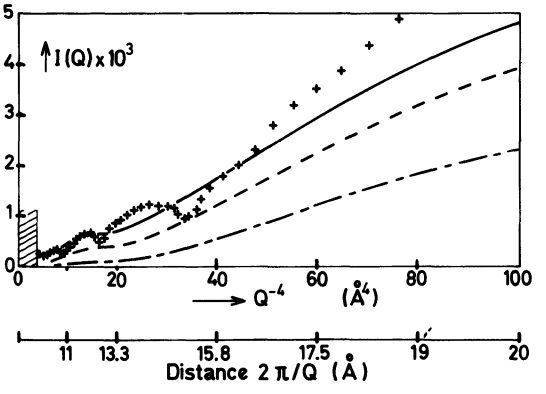

Fig. 11. — Asymptotic trend at high Q for SDS-p_{25} in D_2O; data from D16. Full line : fit by polydisperse spheres with sharp boundaries. - - - - fit by polydisperse spheres with staircase boundaries, $2e = 2$ Å; —·— same, $2e = 4$ Å. In each case the average volume of the spheres is fixed to match the measured aggregation number of SDS micelles.

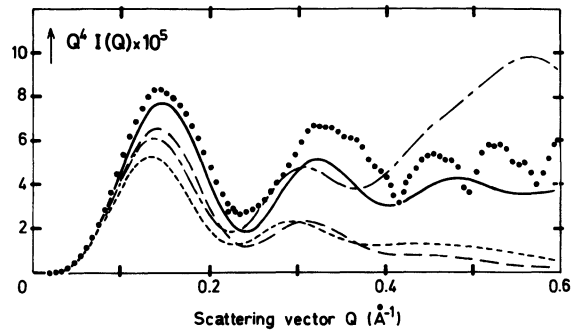

Fig. 12. — Oscillation patterns for spheres with diffuse boundaries (- - - $2e = 2$ Å, ——— $2e = 4$ Å) and for spheres with cavities plus diffuse boundaries (- — -, $2e = 2$ Å) compared with the data from D16. The mismatch at $Q = 0.15$ indicates that, for identical aggregation numbers, the SDS micelles are much more compact than such porous spheres.

this core appears as a homogeneous volume, and its internal structure is not resolved. For this reason it is necessary to label specifically some groups on the hydrocarbon chains of SDS. In this section we consider the distances between end groups (CD_3), and those between the methylene groups in the third position beyond the head (γCD_2).

In our first attempt to measure these distances [52], we tried to obtain conditions where the scattering would be dominated by the labelled groups; for this we used SDS-12d_3 in H_2O. This choice was not good, since the large incoherent scattering by H_2O swamps the coherent scattering beyond $Q = 0.2$ Å^{-1}; also the polar groups are not matched by H_2O, and their contribution must still be extracted from a comparison with unlabelled micelles.

The scattering from labelled micelles in D_2O yields a much better signal to noise ratio; figure 13 shows their scattering curves, plotted as $Q^4 I(Q)$ *vs.* Q in order to emphasize the high Q region where they differ the most from regular micelles. With D_2O as a solvent, however, the contributions from the labelled groups are small compared with those from the rest of the micelle; small errors in the modelization of the micelles can easily mask the effects of the labelled groups.

This is demonstrated in figures 14 and 15, where the data are compared with theoretical predictions for labelled and for unlabelled micelles. Here large differences between the data and some of the predictions appear around the 2nd maximum of the IQ^4 plot. However these differences may well be produced by an incorrect distribution of micellar sizes, or an inadequate modelling of the polar layer; conversely the agreement of some theoretical curves with the data is fortuitous.

It is therefore necessary to extract from the data a structural information concerning the labelled groups alone. Now the scattered *amplitudes* can always be decomposed into contributions of head groups, core,

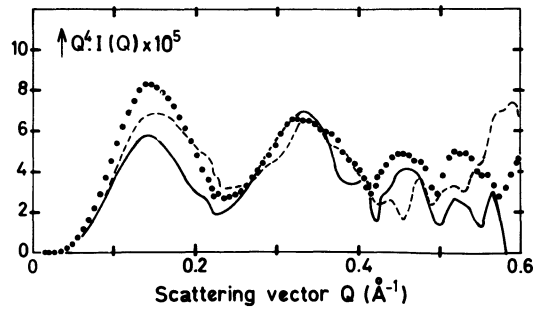

Fig. 13. — Scattering curves of labelled micelles at high contrast, corrected and rescaled as explained in section 3. Dots : SDS-p_{25} in D_2O. Full line : SDS-12d_3 in D_2O. Dashed line : SDS-3d_2 in D_2O.

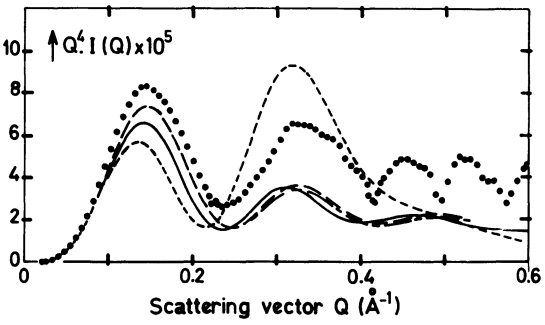

Fig. 14. — Fits at high contrast for unlabelled micelles. Dots : data from D16 for SDS-p_{25} in D_2O. ——— : from Gruen [26], - - - : from Gruen without the constraint of constant hydrocarbon density. – – – : from Cabane [40] with CH_3 dispersed throughout the core. – – – : from Cabane with CH_3 concentrated near the centre.

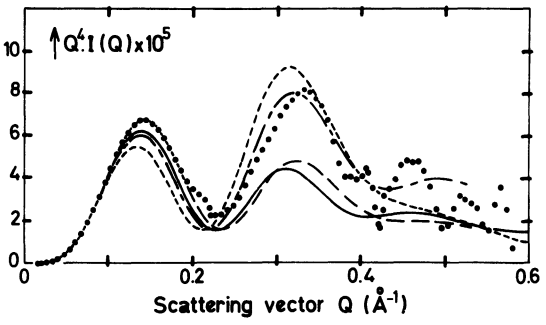

Fig. 15. — Fits a high contrast for labelled micelles. Dots : data from D16 for SDS-12d_3 in D_2O. Fits : as in figure 14.

and labelled groups :

$$A = A_1 + A_2 + A_3 . \qquad (9)$$

If the scattered amplitudes corresponding to labelled and unlabelled micelles could be measured and subtracted, then the contribution from the labelled groups could be isolated. However, in the scattered intensities,

their contributions are mixed with the others by crossed terms which describe correlations between different groups :

$$I = \langle A_1 . A_1^* \rangle + \langle A_1 . A_2^* \rangle + \cdots \qquad (10)$$

To proceed further it is necessary to follow the method of Bendedouch, Chen and Koehler [14], who assume that the average scattered amplitude can be calculated as a square root of the intensity. This is in general not true, because the thermal fluctuations and the rotational motions of the micelles are averaged out in the average amplitude $\langle A \rangle$, whereas they contribute to the intensity :

$$I = \langle A . A^* \rangle \neq \langle A \rangle^2 . \qquad (11)$$

However the discussion of fluctuations presented in § 2.3 shows that this assumption will be acceptable at low resolution, where the micelles can be considered as being all identical and spherical. Then the amplitude scattered by the CD_3 groups alone can be calculated through :

$$A_{CD_3}(Q) = \varepsilon \sqrt{I_{12d_3}(Q)} - \varepsilon' \sqrt{I_{p_{25}}(Q)} \qquad (12)$$

where ε and ε' are both equal to + 1 at low Q. Subsequently this amplitude is Fourier transformed to yield a radial distribution for the methyl groups within the micelle. The best resolution which can be achieved for this distribution corresponds to Q values near the first minimum of the scattering curves, i.e. $Q_{max} = 0.2$ Å^{-1}, or in real space $R = 15$ Å ; details finer than this spacing are not seen at this level. This is emphasized in figure 16, where 2 different radial distributions have been transformed into scattered amplitudes, truncated at Q_{max}, and then transformed back into real space : the density profiles obtained with a truncation at 0.24 Å^{-1} bear no resemblance to the original ones.

For higher resolutions, and therefore larger Q values,

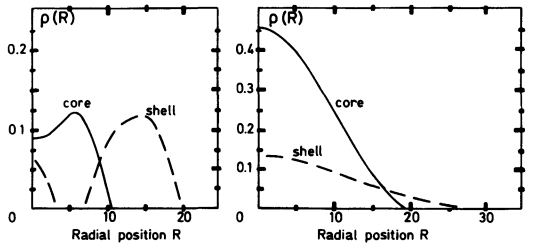

Fig. 16. — Effect of a truncation of the scattering curves on calculated radial profiles of scattering density. The original particles are a spherical core, $R = 9.2$ Å, with a uniform density, and a spherical shell, also of uniform density between $R = 9.2$ Å and 18.4 Å. Left : the calculated scattering curves have been truncated at $Q_m = 1$ Å^{-1}, and then retransformed into R space. Right : same, but truncated at $Q_m = 0.24$ Å^{-1}.

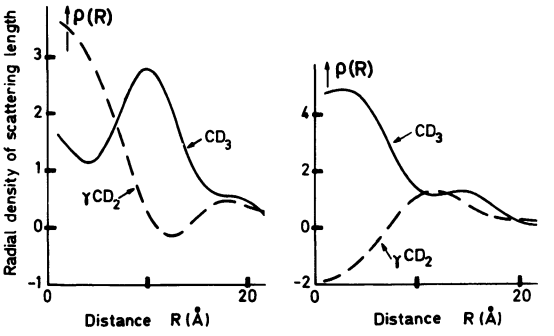

Fig. 17. — Left : radial profiles of scattering density, obtained from the difference between the « amplitudes » scattered by labelled and unlabelled micelles. The signs of the « amplitudes » have been taken as positive through the whole range of Q. This yields unphysical locations for the labelled CD_3 and γCD_2 groups. Right : same as above, but the signs of the amplitudes are reversed at $Q = 0.22$ Å^{-1}. The average locations of the labelled groups are found correctly, but the profiles are still severely distorted.

the use of equation (12) can lead to serious errors, because the phases ε and ε' of the experimental amplitudes are not known. Figure 17a shows the effect of a wrong choice for these signs, while figure 17b indicates that even with a better choice the results will never be very good. In fact, it is only for nearly spherical particles, such as lattices, some lipoproteins or some viruses, where the intensity curve shows at least 5 consecutive oscillations, that the amplitudes can be recovered with no ambiguity on their signs [43].

Basically, these problems arise from trying to determine *radial locations* for the labelled groups; indeed scattering does not measure intrinsic positions but *distances between scatterers.* Accordingly, the errors produced by the indiscriminate use of equation (12) can be minimized if the amplitude differences are squared prior to the Fourier transform, yielding the average distributions of distances $P(r)$ between labelled groups. The errors made in this procedure can be checked with an arbitrary distribution of labelled groups in a model micelle. Firstly the scattering from the labels only is calculated directly from this distribution, assuming a 40 % dispersion in the volumes of the micelles; this is Fourier transformed to give the exact distribution of distances between labelled groups. Secondly the scattered intensities for labelled and unlabelled micelles are calculated and used to obtain the pseudo-amplitude for the labels alone through equation (12); the signs ε and ε' are not known, but assumed to be identical; this pseudo-amplitude is then squared and transformed to yield the approximate distribution of distances. As shown in figure 18, this is fairly close to the correct distribution; a slight regression towards the distribution of the whole micelle shows up because of the fluctuations in micellar volumes.

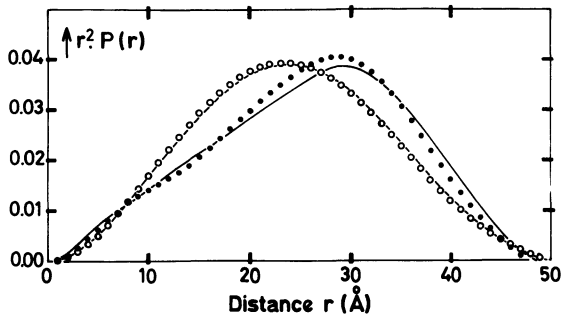

Fig. 18. — Simulation of the errors made in calculating the distribution of distances between labelled groups. Circles : distribution of distances within polydisperse homogeneous spheres. Dots : distribution of distances between labelled points in a shell within each sphere. Solid line : indirect calculation of the distribution of distances between labelled points by comparing the scattering from labelled and unlabelled spheres. Because the spheres are polydisperse, this method is not exact and produces a slight regression of the calculated distribution of labels towards the distribution of distances of the unlabelled sphere.

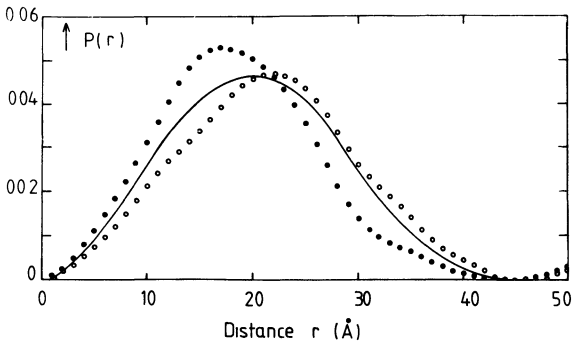

Fig. 19. — Distribution of distances within SDS micelles, calculated from the D16 data. Solid line : unlabelled micelles. Dots : distances between CD_3 groups only. Circles : γCD_2 groups (3d methylene from head). If all CD_3 groups were concentrated near a « centre », their distribution would peak at 10 Å, and its longest distances would be close to 20 Å. If the γCD_2 groups were confined to a spherical shell, their distances would give a triangular distribution, with a peak near 27 Å and a largest distance near 40 Å.

6.2 MEASURED DISTRIBUTIONS OF DISTANCES. — Since this method gives good results for spherical particles with a 40 % polydispersity in volumes, it can be used to determine the actual distributions of distances for CD_3 and γCD groups in SDS micelles. These distributions are shown in figure 19, together with the average distribution of distances for the whole unlabelled micelle. They are surprisingly close to each other : *the most probable distance* is 17 Å for the CD_3, 20 Å for the whole micelle and 22 Å for the γCD_2; in each case the *longest chord* is 40 Å, equal to the micellar diameter determined from $\overline{N}$ and from the period of the oscillations of $I(Q)$. Thus the chain ends are not concentrated near a « centre » of the micelle, and the γCD_2 do not remain in a spherical shell.

All the currently available models for the internal structure of the micelle fail to reproduce this striking behaviour (Fig. 20). As a rough measure of this discrepancy, consider the ratio of the average distance between CD_3 groups to the average distance within the whole core, whose value is 0.85 according to our data. This ratio is predicted to be 0.45 in a model which maximizes the concentration of end groups near the « centre » (40), 0.58 in a spherical average of Fromherz's micelle [37], 0.65 in Dill and Flory's interphase theory [28] as well as in a simple model which disperses the end groups throughout the core [40], 0.71 in Gruen's theory [26], and 0.78 in a modification of this theory where the constraint of constant density in the core is released. These discrepancies are large, and cannot be explained by the slight regression mentioned above, which would only shift the experimental value by 2 %. Another rough test is provided by the ratio of the average distance between γCD_2 groups to the average distance within the core : according to our data this ratio is equal to 1.1. Yet it is predicted to be 1.2 according to the spherical average of Fromherz's micelle, 1.2 and 1.25 in the simple models of [40], 1.29 in Gruen's theory, and 1.17 when the constraint of constant hydrocarbon density is released.

At first sight, a way out seems to be suggested by the fact that releasing the constraint of uniform hydrocarbon density does improve the fit; this would point to a fuzzy structure with massive interpenetration of water and hydrocarbon. This is misleading, since this improvement is obtained by letting the hydrocarbon density become *higher* than that of liquid hydrocarbons in some shells of the core, and lower in others; if it is constrained to remaining equal or below that of bulk hydrocarbons, the penetration of water would swell the core; this is ruled by our data on unlabelled micelles (§ 5.1 and 5.2). Releasing this constraint is also rather unreasonable, since the cost of water/hydrocarbon contacts is by far the largest free energy in amphiphilic solutions.

The other constraint which is common to most theories is that of a spherical geometry. This constraint may well be a major shortcoming of the models. Indeed the fluctuations in the volumes, or aggregation numbers of micelles are on the order of $\sigma/\overline{N} = 0.33$ (§ 5.1); it would be surprizing if the fluctuations of their shape were smaller than this. Moreover the Monte Carlo simulations of Pratt and coworkers [38, 39], where the amphiphilic molecules are placed on a uniform lattice, produce amphiphilic aggregates with very irregular shapes.

Our experimental distributions of distances between labels support this idea of significant shape fluctuations away from the spherical geometry. Indeed shape fluctuations with the $l = 2$ symmetry, especially those

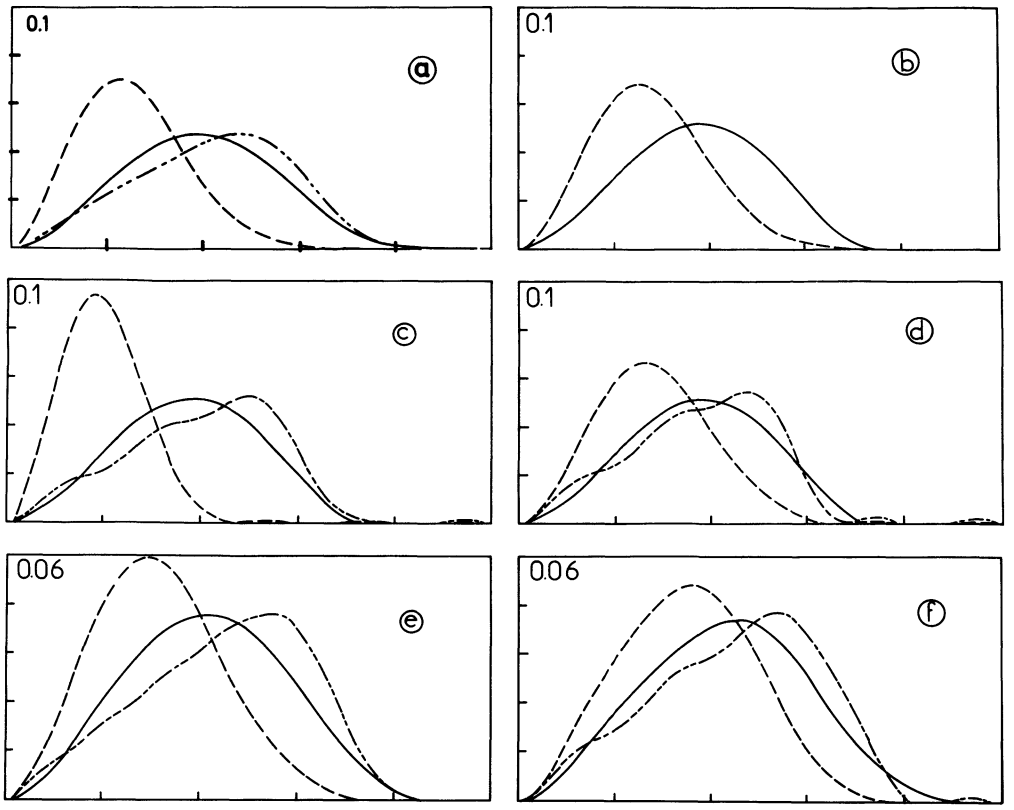

Fig. 20. — Theoretical predictions for the distribution of all distances within the core (———), that between CD_3 end groups (———), and that between γCD_2 groups (- — -). (a) Fromherz [37]. (b) Dill and Flory [28]. (c) Cabane [40] with end groups near centre. (d) Cabane with end groups dispersed through the core. (e) Gruen [26]. (f) Gruen without the constraint of constant hydrocarbon density. All these models predict the CD_3 to be closer to each other, and the γCD_2 further from each other than the data.

which deform the micelle towards a shape similar to those of red blood cells, would bring some end groups away from the centre and some head groups near the centre of the micelle. Consequently the distributions of distances between labelled groups would regress towards that for the whole core, reducing the discrepancy observed in the spherical geometry. A more subtle effect is that such fluctuations would contribute to the crossed terms between the labelled groups and the core (see Eq. (10)); this might also result in an apparent regression of the distributions for labelled groups towards that for the whole core.

7. Conclusions.

The structures of SDS micelles in water have been observed through static small angle scattering, with a resolution $\pi/Q_{max} = 5$ Å; they can be described as follows :

a) The *average structure* consists of 74 molecules clustered in a dense sphere. Other *simple* shapes, e.g. ellipsoids, cubes do not fit the data in the range $0.2 < Q < 0.4$ Å^{-1}.

b) *Fluctuations* are so important that at any given time most micelles deviate substantially from the average structure. A measure of these deviations is given by the damping of the oscillations in the single micelle scattering curve : this corresponds to a standard deviation of 40 %. A large fraction of these deviations from the average structure is made of fluctuations in the micellar aggregation numbers, or volumes. A thermodynamic analysis, and also the direct evidence from electron microscopy, point to a deviation $\sigma_N/\overline{N} = 0.33$; this is consistent with our data. Another fraction of these deviations must correspond to fluctuations in the shapes of the micelles; of these, the most important are probably the lowest order spherical harmonics, i.e. $l = 2$. These shape fluctuations have a minor effect on the scattering at high core/solvent contrast, but a major one at low contrast, when the internal structure of the core is resolved (see below).

c) *Water/hydrocarbon contact.* The core is limited by a boundary which is sharp at the resolution level of the experiment, i.e. its full width is well below 5 Å. The volume which is inside this boundary has an average radius of 18.4 Å; this dimension matches

precisely the hydrocarbon volume of 74 SDS molecules; hence water penetration inside this volume must be very small, in any case less than one water molecule per SDS molecule. Water/hydrocarbon contact is therefore limited to the surface of the core; still this wetting of the surface provides a substantial hydration of the hydrocarbon, since one quarter of the core's volume lies in a surface layer of thickness 1.5 Å.

d) The *internal structure of the core* is observed through experiments on SDS labelled with deuterium on specific methyl (ω) or methylene (γ) groups. The distribution of distances between CD_3 end groups has been measured : it is close to that for the whole core; the distribution of distances between γCD_2 groups has been found to be even closer to the distribution of all distances within the core. Any structural model which concentrates the end groups near a « centre » of the micelle and the γCD_2 in a spherical shell, as in the pervasive textbook picture [32, 33] fails spectacularly. Theories which distribute the end groups throughout the core while maintaining a constant hydrocarbon density within the core and keeping the heads on a spherical shell fare somewhat better, the smallest mismatch being provided by Gruen's model. Nevertheless all such models which retain a fixed spherical geometry will produce micelles where the end groups are too close to each other, and the outer CD_2 groups too far apart compared to our data; the only way out seems to be to allow large shape fluctuations, especially those with the $l = 2$ symmetry. This conclusion is in agreement with the Monte Carlo simulations of Pratt, Owenson and Sun [65] which show very irregular shapes for computer generated amphiphilic aggregates.

e) Many of these problems can be traced back to the original description of micelles as *invariant particles*, as opposed to a more general description of spatial fluctuations in the concentrations of DS^- and Na^+ ions in the solution [62]. The concept of invariant particles reduces all such fluctuations to the existence of a set of well defined particles; in a second stage, fluctuations away from the average structure are allowed. At low resolution this method is very powerful, as it allows the use of thermodynamics to treat interparticle interactions — this is the one component macrofluid concept [58] — and of crystallographic techniques to resolve the single particle structure. Yet this method is appropriate only when the fluctuations are small at the resolution level of the data. For SDS the results of this method are good at a resolution of 15 Å because the SDS micelles are not very polydisperse. However at high resolution (5 Å) the fluctuations become much more important, and the invariant particle concept fails, as evidenced by the fact that the distribution of distances between end groups, or that for methylene groups, are not compatible with a fixed geometry.

A move back to the general description based on correlation functions only would be too drastic, and probably useless as a structural tool. It may be more appropriate to describe micelles as small pieces of amphiphile/water interfaces, with topological constraints (closed surfaces with no edges) but no geometric constraints (no particular shape preferred). In this respect SDS micelles are a remarkable intermediate case between : (i) larger objects with a complex internal organization such as aggregates of micelles bound to a macromolecule [61] or biological particles [43, 44], where the invariant particle concept works quite well because the fluctuations in mass or composition are very small; (ii) aggregates of very short amphiphiles, non amphiphilic self assembling systems, and some multicomponent micelles [66], where very large mass or composition fluctuations can take place, making the description of an average structure meaningless. This choice of an appropriate level of description may be a general problem for all self assembling systems.

Acknowledgments.

The SDS labelled by deuterium in the γ position has been synthesized by C. Germain in Orsay; the purity of this SDS was a crucial factor in the comparisons between labelled and unlabelled micelles. We thank J. B. Hayter for making available to us the programs which calculate the intermicellar structure factor and D. W. R. Gruen for sending us some results of his calculations prior to publication. The scattering experiments were performed at ILL in Grenoble, France; it is a pleasure for us to acknowledge the material help and advice from ILL staff members, including M. Rawiso, P. Timmins, S. Wilson, D. Worcester and G. Zaccai. This work was supported by the « Greco Microémulsions » and by the PIRSEM of CNRS.

Appendix 1.

2 SHELL MODEL FOR THE SDS MICELLE. — Many scattering experiments on surfactant solutions have been interpreted by considering a model where the micelle is made of 2 concentric spherical shells : a hydrocarbon core of uniform density ρ_c and a polar shell of uniform density ρ_p. Typically this polar layer will contain the head groups (OSO_3^-), most counterions (Na^+), the first methylene group of every chain (αCH_2), and all the hydration water, i.e. about 8 water molecules per SDS molecule. This model is used in § 4 to analyse our low resolution data on SDS-p_{25} in D_2O and on SDS-d_{25} in H_2O. The corresponding radii and scattering densities are as

follows :

Micellar solution	R_c	ρ_c	$\rho_c - \rho_s$	R_p	ρ_p	$\rho_p - \rho_s$	ρ_s
SDS-p_{25}/D_2O	17.85	−0.41	6.67	22.78	5.67	0.59	6.26
SDS-d_{25}/H_2O	17.40	6.9	7.46	22.21	1.03	1.59	−0.56

R_c radius of hydrocarbon core, in Å
R_p outer radius of polar layer
ρ_c scattering density of core in $cm^{-2} \times 10^{10}$
ρ_p scattering density of polar layer
ρ_s scattering density of the solvent, H_2O or D_2O.

However many other 2 shell models, or a single shell model can fit the data just as well. This is obvious at low resolution ($Q_{max} = 0.2$ Å^{-1}) because the spacing of points in r space (15 Å) is then wider than the thickness of the outer shell. At high Q, these models could be distinguished if the micelles were all spherical and identical; however the fluctuations in their sizes and shapes make this separation difficult; for example, a change in the distribution of sizes can, to some extent, compensate for a change in internal structure. Experiments on labelled micelles are necessary to lift this ambiguity (§ 6).

Nevertheless, such models are useful because their scattering can be calculated through simple formulae. The $Q \to 0$ limit of the scattered intensity is :

$$\langle | A_1(Q \to 0) |^2 \rangle = [V_c(\rho_c - \rho_s) + V_p(\rho_p - \rho_s)]^2 . \quad (13)$$

With the choice of core and polar layer given above, the term due to the core only is 10 times larger than the crossed term between the core and the polar layer. However at high Q there is no such crossed term, as can be seen from the expression for Porod's invariant :

$$P(r = 0) = \frac{K}{2\pi^2} \int_0^{Q_{max}} Q^2 I(Q)\, dQ =$$

$$= V_c(\rho_c - \rho_s)^2 + V_p(\rho_p - \rho_s)^2 \quad (15)$$

or for Porod's limit :

$$\left.\frac{dP}{dr}\right|_{r=0} = K \lim_{Q \to \infty} Q^4 I(Q) = A_{cp}(\rho_c - \rho_p)^2 + A_{ps}(\rho_p - \rho_s)^2 . \quad (16)$$

With the same choice of core and polar layer, the contribution of the polar layer is 100 times smaller than that of the core; with a denser polar layer it would be somewhat larger, up to one-tenth of that from the core.

In conclusion, the polar regions of the SDS micelle contribute little to the scattering observed at high contrast between core and solvent. The asymptotic limit of $I(Q)$ is effectively controlled by the largest discontinuity in scattering density, which occurs at the core's surface. The $Q \to 0$ limit and the integral of the scattered intensity measure essentially the volume of the core; the ratio of these 2 quantities is the value of this volume, measured in absolute units; the aggregation numbers for the SDS micelle shown in table II, column c, are calculated from this value. Of course this last method would fail if the polar region of the micelle was more important, as would be the case for some non ionic micelles.

References

[1] WILLIAMS, R. J., PHILLIPS, J. N., MYSELS, K. J., *Trans. Faraday Doc.* **51** (1955) 728.
[2] MYSELS, K. J., *J. Colloid Sci.* **10** (1955) 507.
[3] MYSELS, K. J., PRINCEN, L. H., *J. Phys. Chem.* **63** (1959) 1696.
[4] TARTAR, H. V., LELONG, A. L. M., *J. Phys. Chem.* **59** (1956) 1185.
[5] KUSHNER, L. M., HUBBARD, W. D., *J. Colloid Sci.* **10** (1955) 428.
[6] ANACKER, E. W., RUSH, R. M., JOHNSON, J. S., *J. Phys. Chem.* **68** (1964) 81.
[7] LIANOS, P., ZANA, R., *J. Colloid Interface Sci.* **84** (1981) 100.
[8] REISS HUSSON, F., LUZZATI, V., *J. Colloid Interface Sci.* **21** (1966) 534.
[9] REISS HUSSON, F., LUZZATI, V., *J. Phys. Chem.* **68** (1964) 3504.
[10] CABOS, C., DELORD, P., *J. Physique* **39** (1978) 432.
[11] CABOS, C., DELORD, P., *J. Physique Lett.* **38** (1977) L-365.
[12] HAYTER, J. B., PENFOLD, F., *J. Chem. Soc. Faraday Trans I* **77** (1981) 1851.
[13] HAYTER, J. B., PENFOLD, F., *Colloid Polym. Sci.* **261** (1983) 1022.
[14] BENDEDOUCH, D., CHEN, S. H., KOEHLER, W. C., *J. Phys. Chem.* **87** (1983) 153.

[15] BENDEDOUCH, D., CHEN, S. H., KOEHLER, W. C., *J. Phys. Chem.* **87** (1983) 2621.
[16] HARTLEY, G. S., *Aqueous Solutions of paraffin chain salts* (Hermann, Paris) 1936.
[17] TANFORD, C., *The hydrophobic effect* 2nd ed. (Wiley, New York) 1980.
[18] WENNERSTRÖM, H., LINDMAN, B., *Phys. Rep.* **52** (1979) 1.
[19] LINDMAN, B., WENNERSTRÖM, H., *Top. Curr. Chem.* **87** (1980) 1.
[20] WENNERSTRÖM, H., LINDMAN, B., *J. Phys. Chem.* **83** (1979) 2391.
[21] ISRAELACHVILI, J. N., MITCHELL, D. J., NINHAM, B. W., *J. Chem. Soc. Faraday Trans. 2* **72** (1976) 1525.
[22] MITCHELL, D. J., NINHAM, B. W., *J. Chem. Soc. Faraday Trans 2* **77** (1981) 601.
[23] GRUEN, D. W. R., *J. Colloid Interface Sci.* **84** (1981) 281.
[24] GRUEN, D. W. R., DE LACEY, E. M. B., in *Surfactants in solution,* Mittal, K. and Lindman, B. Ed (Plenum) 1984.
[25] GRUEN, D. W. R., private communication.
[26] GRUEN, D. W. R., *J. Phys. Chem.* **89** (1985) 146.
[27] BEN SHAUL, A., SZLEIFER, I., GELBART, W. M., *Proc. Nat. Acad. Sci.* **81** (1984) 4601.
[28] DILL, K. A., FLORY, P. J., *Proc. Nat. Acad. Sci.* **78** (1981) 676.
[29] DILL, K. A., *J. Phys. Chem.* **86** (1982) 1498.
[30] DILL, K. A., in *Surfactants in Solution,* op. cit.
[31] DILL, K. A., KOPPEL, D. E., CANTOR, R. S., DILL, J. D., BENDEDOUCH, D., CHEN, S. H., *Nature* **309** (1984) 42.
[32] MENGER, F. M., *Acc. Chem. Res.* **12** (1979) III.
[33] MENGER, F. M., JERKUNICA, J. M., JOHNSTON, J. C., *J. Am. Chem. Soc.* **100** (1978) 4676.
[34] MENGER, F. M., in *Surfactants in Solution,* op. cit.
[35] FROMHERZ, P., *Chem. Phys. Lett.* **77** (1981) 460.
[36] FROMHERZ, P., *Ber. Bunsenges Phys. Chem.* **85** (1981) 537.
[37] FROMHERZ, P., in *Surfactants in solution,* op cit.
[38] HAAN, S. W., PRATT, L. R., *Chem. Phys. Lett.* **79** (1981) 436.
[39] OWENSON, B., PRATT, L. R., *J. Phys. Chem.* **88** (1984) 2905.
[40] CABANE, B., *J. Physique* **42** (1981) 847.
[41] ZEMB, T., CHACHATY, C., *Chem. Phys. Lett.* **88** (1982) 68.
[42] ZEMB, T., CHACHATY, C., in *Surfactants in solution,* op. cit.
[43] JACROT, B., *Rep. Progr. Phys.* **39** (1976) 911.
[44] STUHRMANN, H. B., MILLER, A., *J. Appl. Cryst.* **11** (1978) 325.
[45] GUINIER, A., FOURNET, G., *Small angle X ray scattering* (Wiley) 1955.
[46] VAN BEURTEN, P., VRIJ, A., *J. Chem. Phys.* **74** (1981) 2744.
[47] CABANE, B., in *Colloides et Interfaces* (Editions de Physique) 1984.
[48] KOTLARCHYK, M., CHEN, S. H., *J. Chem. Phys.* **79** (1983) 2461.
[49] HAYTER, J. B., in *Physics of amphiphilis : micelles, vesicles and microemulsions.* V. Degiorgio and M. Corti, eds. (Italian Physical Society and North Holland) 1985.
[50] LUZZATI, V., TARDIEU, A., *Ann. Rev. Biophys. Bioeng.* **9** (1980) 1.
[51] TABONY, J., *Mol. Phys.* **51** (1984) 975.
[52] CABANE, B., DUPLESSIX, R., ZEMB, T., in *Surfactants in Solution,* op. cit.
[53] SAFRAN, S., *J. Chem. Phys.* **78** (1983) 2073.
[54] LJUNDGGREN, S., ERIKSSON, J. C., *J. Chem. Soc. Faraday Trans. 2* **80** (1984) 489.
[55] However, for the lowest Q value of D_{16}, $\Delta Q/Q$ = 30 % FWHM due to divergence. At the peak in $I(Q)$ this is reduced to 10 %.
[56] The incoherent scattering from H_2O drops beyond 0.7 $Å^{-1}$ due to inelastic effects.
[57] Hayter, J. B., Penfold, J., *Mol. Phys.* **42** (1981) 109.
[58] HANSEN, J. P., HAYTER, J. B., *Mol. Phys.* **46** (1982) 651.
[59] HAYTER, J. B., ZEMB, T., *Chem. Phys. Lett.* **93** (1982) 91.
[60] CABANE, B., ZEMB, T., *Nature* **314** (1985) 385.
[61] CABANE, B., DUPLESSIX, R., *J. Physique* **43** (1982) 1529.
[62] EISENBERG, E., *Quat. Rev. Biophys.* **14** (1981) 141.
[63] ZEMB, T., CHARPIN, P., *J. Physique* **46** (1985) 249.
[64] BACHMANN, L., DASCH, W., KUTTER, P., *Ber. Bunsenges Phys. Chem.* **85** (1981) 883.
[65] PRATT, L. R., OWENSON, B., SUN, *Adv. Colloid Interface Sci.,* in press.
[66] ZANA, R., PICOT, C., DUPLESSIX, R., *J. Colloid Interface Sci.* **93** (1984) 43.
[67] CHANG, N. J. and KALER, E. W., *J. Phys. Chem.* **89** (1984) 2996.